Supporting Information

A recyclable metal-organic framework for ammonia vapour adsorption

Tu N. Nguyen,*[a,b] Ian M. Harreschou,[c] Jung-Hoon Lee,[d] Kyriakos C. Stylianou,*[c] Douglas Stephan*[c]

[a] Helen Scientific Research and Technological Development Co., Ltd, Ho Chi Minh City, Vietnam.

[b] Laboratory of Molecular Simulation (LSMO), Institut des Sciences et Ingénierie Chimiques (ISIC), Ecole Polytechnique Fédérale de Lausanne (EPFL Valais), Sion, Switzerland.

[c] Department of Chemistry, Oregon State University, Corvallis, OR 97331, USA.

[d] Computational Science Research Center, Korea Institute of Science and Technology (KIST), Seoul 02792, Republic of Korea

[e] Department of Chemistry, University of Toronto, Toronto, ON M5S 3H6, Canada.

Experimental procedures

General information. All of the chemicals are commercially available and were used without further purification. The organic compound H_3tctb was synthesized based on the reported procedure.[1] Powder X-ray diffraction (PXRD) data were collected on a Bruker D8 Advance using Cu K_α radiation (λ = 1.5418 Å, 50 kW/40mA). Simulated PXRD patterns were generated from the single-crystal data using Mercury 3.7. CO_2 isotherm was collected at 195 K, by gravimetric method using an IGA system (Intelligent Gravimetric Analyser, Hiden Isochema Ltd.). NH_3 isotherms were collected at 303 and 313 K, by gravimetric method on a 90 mg activated sample using the 3Flex system (Micromeritics). Photoluminescence (PL) spectra (excitation at 420 nm) were measured with a Fluorescence Spectrometer LS 55 (PerkinElmer). NMR spectra were collected on a Bruker Advance III 400.

Synthesis of SION105-Eu.[2] 27 mg of H_3tctb and 22 mg of $Eu(NO_3)_3.6H_2O$ were combined in a 4:2 (v/v) mixture of DMF:H_2O in a 10 mL glass vial, and heated to 120°C for 72 hours in an oven. After the reaction, the vials are allowed for cooling down, with the cooling rate of 0.2 °C/min. Resulting rod-shaped colorless crystals were filtered, washed with DMF, soaked in MeOH for 3 days before being filtered again, and then dried in oven at 120 °C.

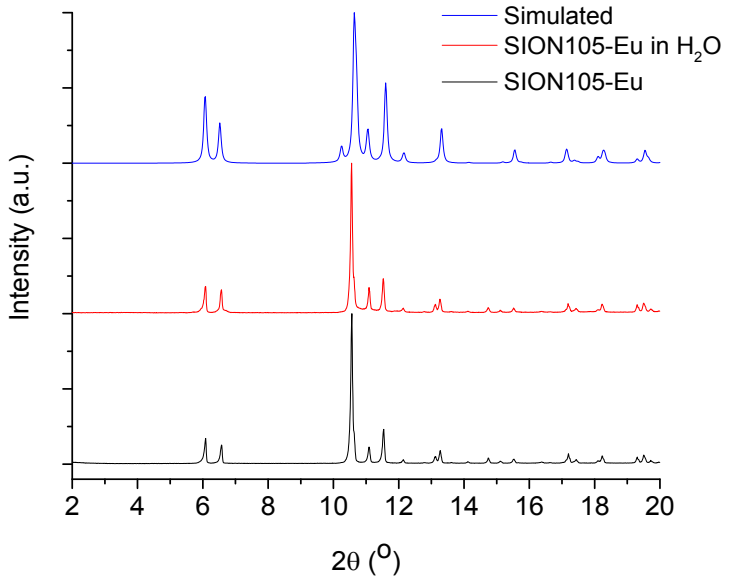

Figure S1. Experimental PXRD patterns of **SION105-Eu** samples (as made and immersed in H_2O), in comparison with the simulated pattern obtained from single-crystal X-ray structure.

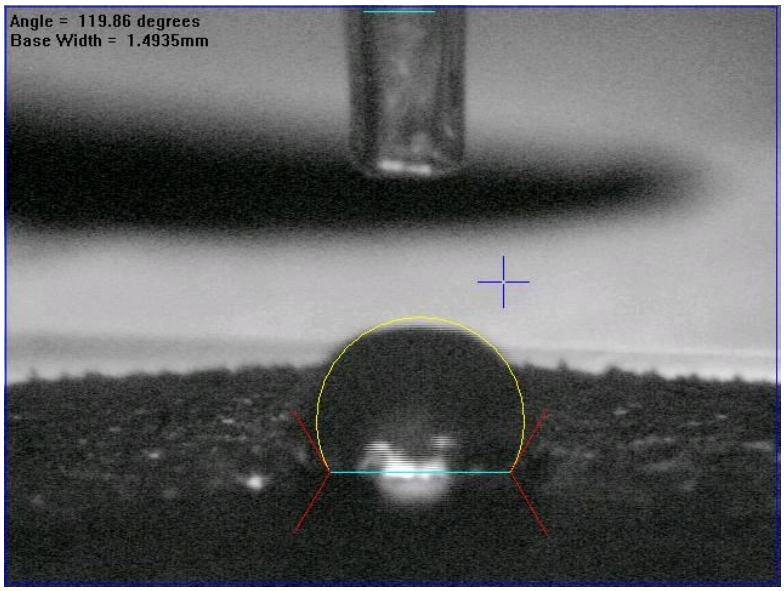

Figure S2. Contact angle measurement of **SION105-Eu**. The angle is 119.86 °, confirming the hydrophobicity of the MOF.

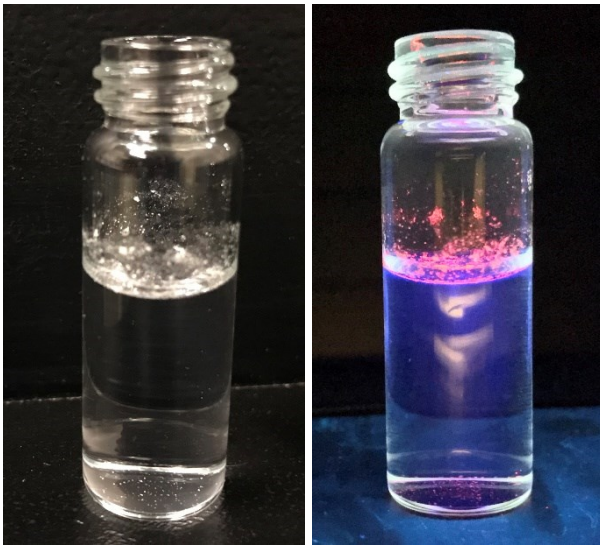

Figure S3. The powder of **SION105-Eu** floats on the top of the water solution in normal condition (left) and under UV radiation (right).

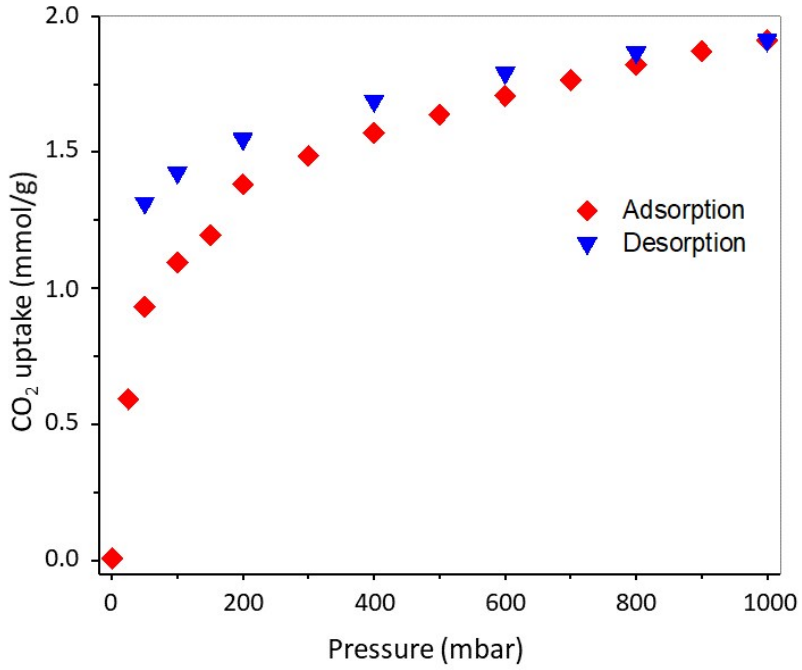

Figure S4. CO_2 adsorption isotherm for **SION105-Eu** collected at 195 K. The BET surface area is 216 m^2/g.

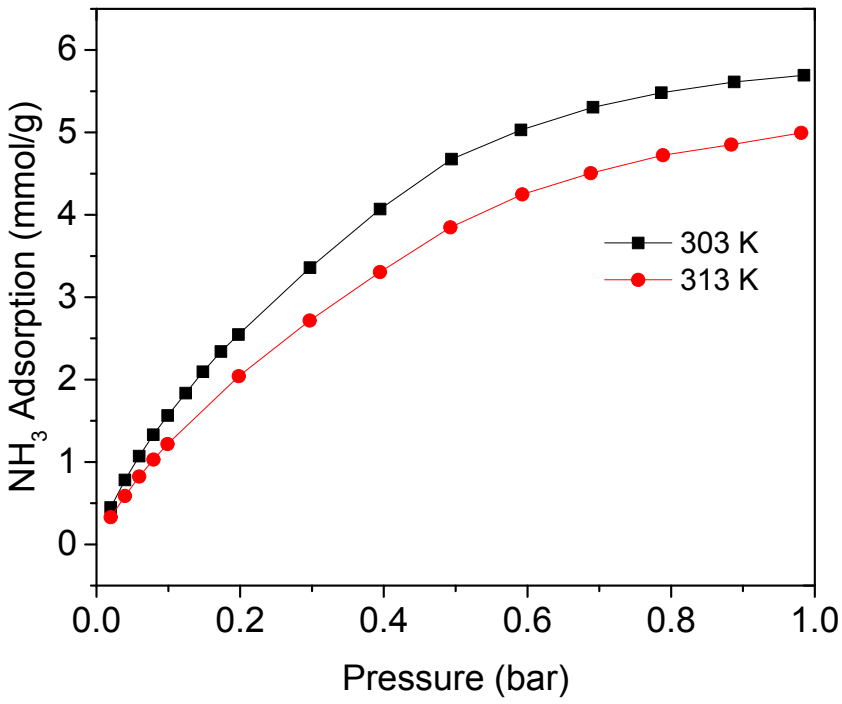

Figure S5. NH_3 adsorption isotherms for **SION105-Eu** collected at 303 and 313 K.

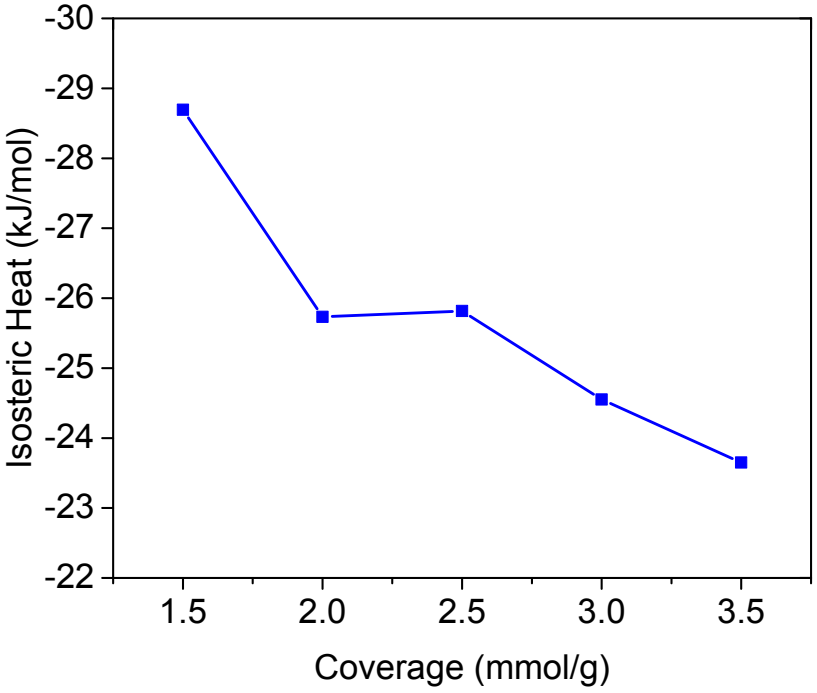

Figure S6. The isosteric heat of NH_3 adsorption calculated based on the Clausius–Clapeyron relation.

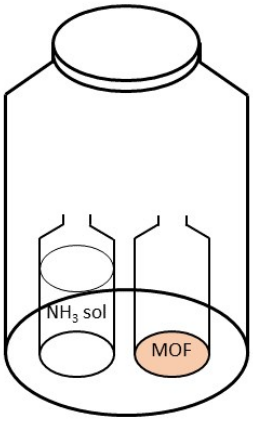

Figure S7. NH_3 vapour adsorption. The cap of the vessel is either tightly closed or loosened.

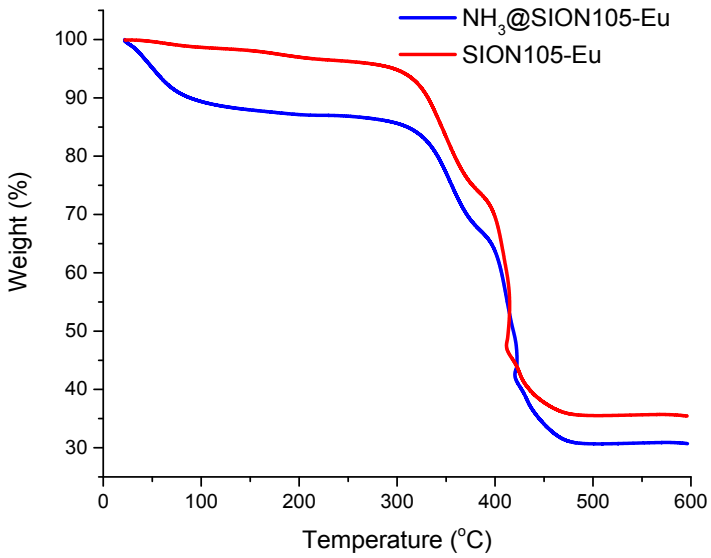

Figure S8. Thermal gravimetric analysis (TGA) profiles of activated **SION105-Eu** and **NH_3@SION105-Eu** (after 6 hours of adsorption). The weight loss of around 10 wt% at below 100 °C corresponds to the release of NH_3.

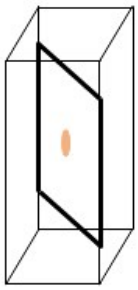

Figure S9. The filter-paper plate is located along the diagonal within the quartz cuvette.

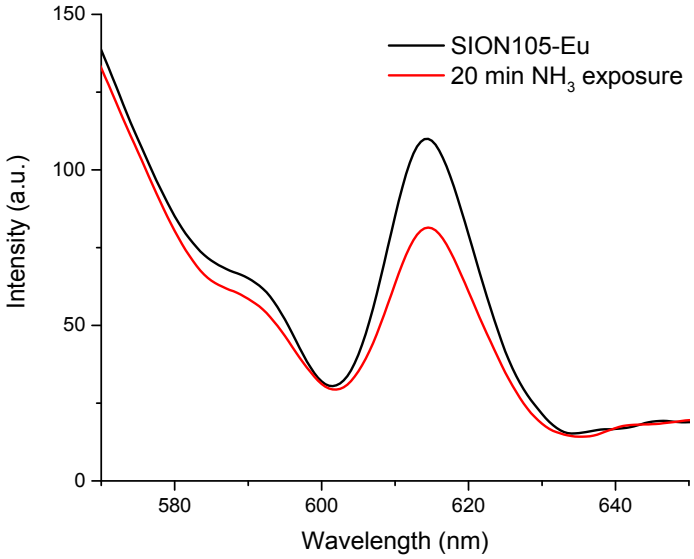

Figure S10. Luminescence quenching of **SION105-Eu** after exposure to NH_3 vapour for 20 min.

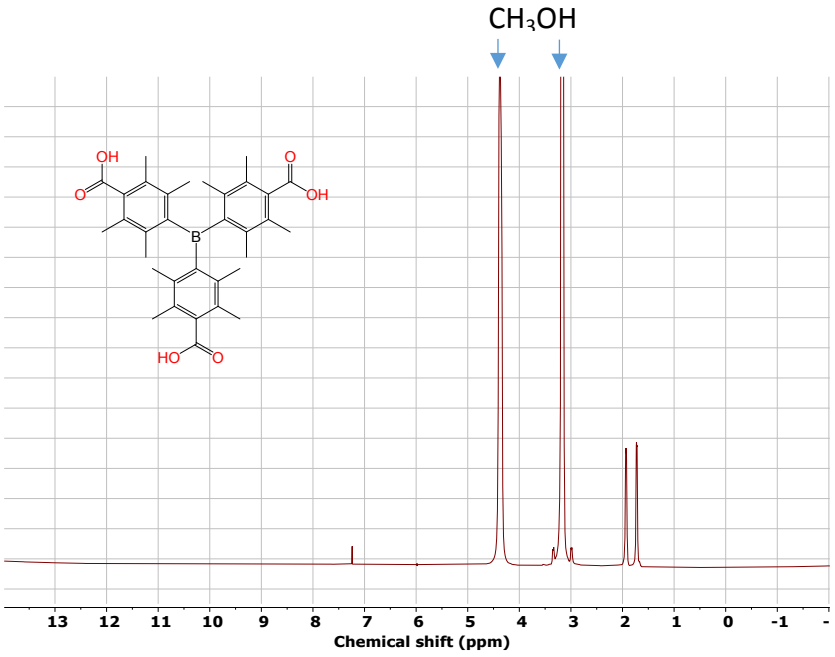

Figure S11. HNMR spectrum of H_3tctb dissolved in $CH_3OH/CDCl_3$.

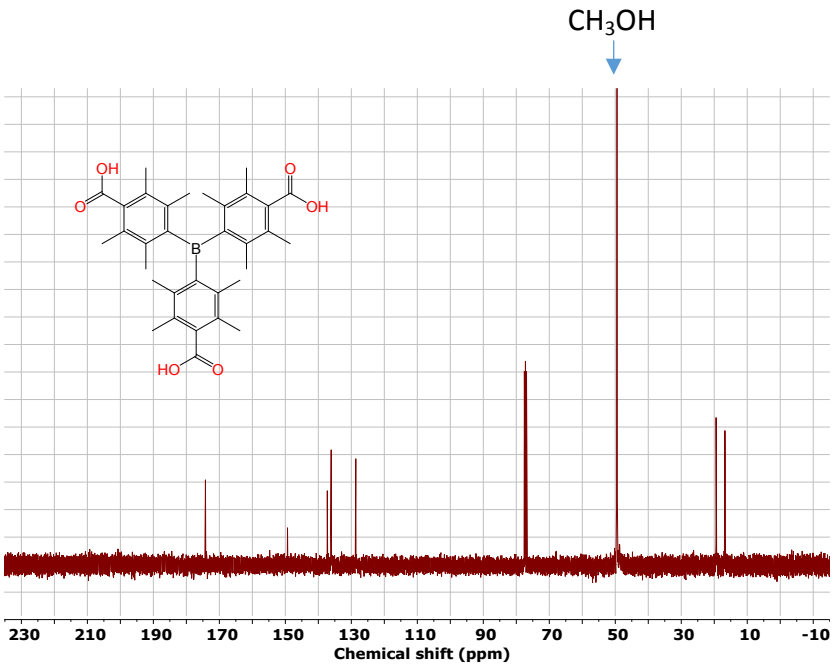

Figure S12. ^{13}C-NMR spectrum of H_3tctb dissolved in $CH_3OH/CDCl_3$.

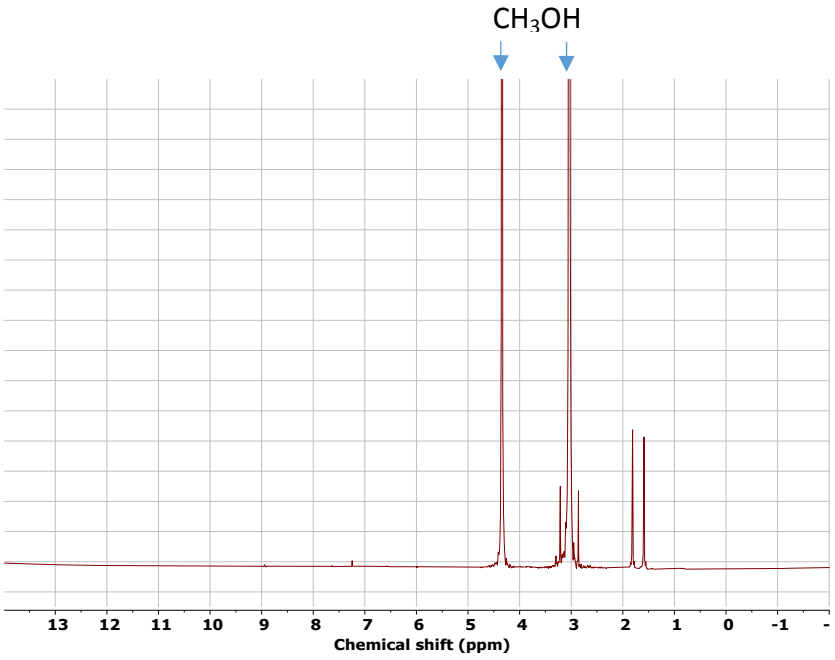

Figure S13. HNMR spectrum of H_3tctb dissolved in $CH_3OH/CDCl_3$ after addition of 10 equivalents of NH_3 (7N in CH_3OH). No dissociation of the ligand was observed.

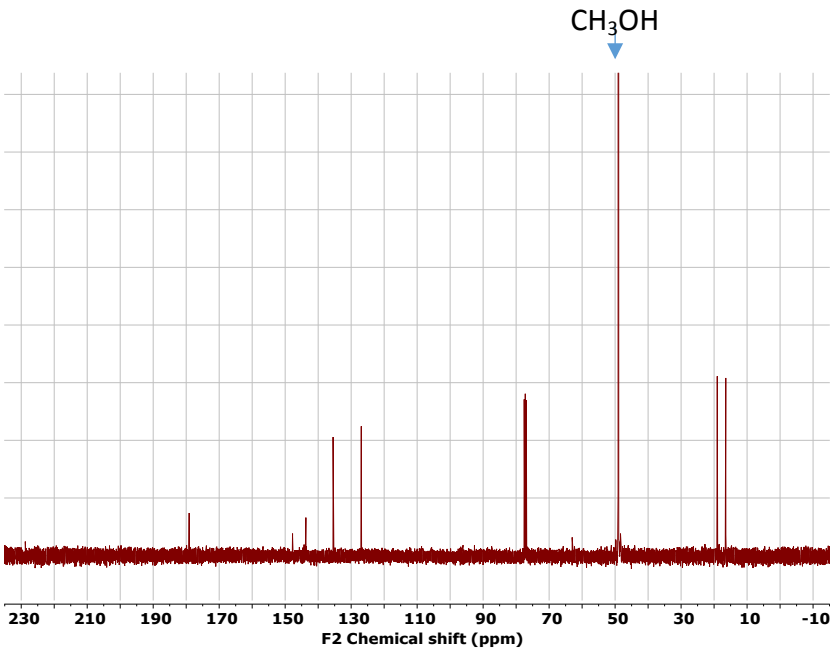

Figure S14. ^{13}C-NMR spectrum of H_3tctb dissolved in $CH_3OH/CDCl_3$ after addition of 10 equivalents of NH_3 (7N in CH_3OH). The downfield shift of the O=C carbon compared to the one of H_3tctb suggesting the deprotonation of the carboxylic groups. No dissociation of the ligand was observed.

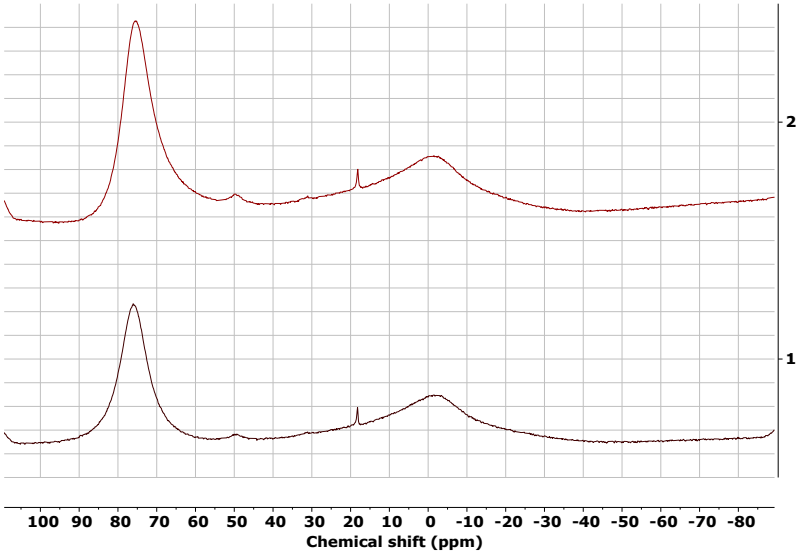

Figure S15. ^{11}B-NMR spectra of Mes_3B before (1) and after (2) adding 10 equivalents of NH_3 (7N in CH_3OH). The broad and strong signals at ~ 75 ppm are characteristic of trigonal planar B. (The broad signal at ~ -3 ppm is due to the presence of B in the glass NMR tube).

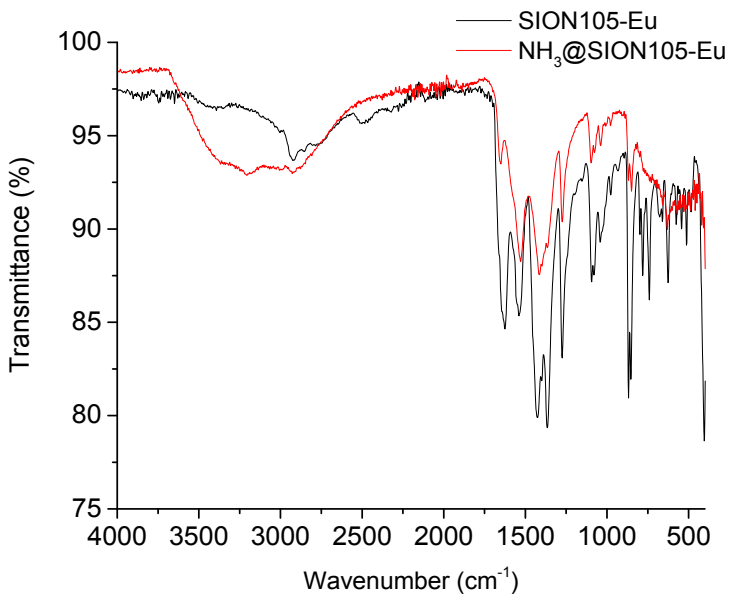

Figure S16. FTIR spectra of **SION105-Eu** before and after 6 hour of NH_3 adsorption (NH_3@**SION105-Eu**).

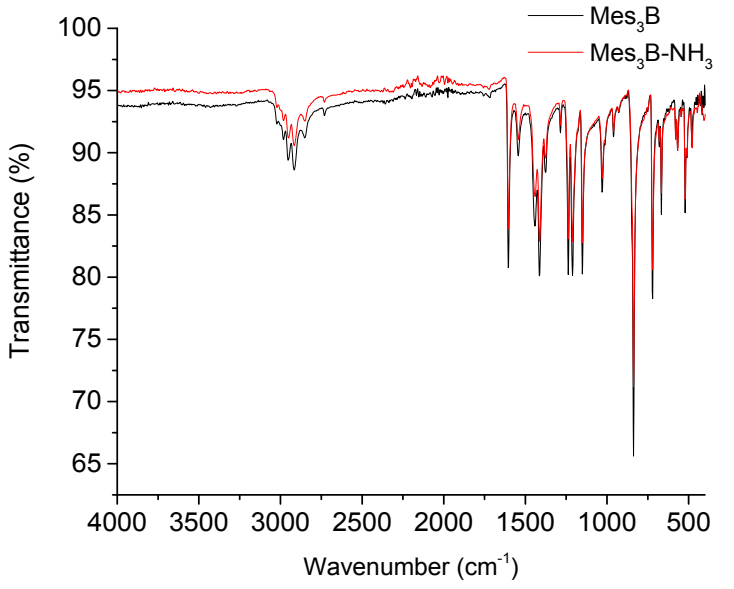

Figure S17. FTIR spectra of Mes_3B before and after 6 hour of NH_3 adsorption (Mes_3B-NH_3).

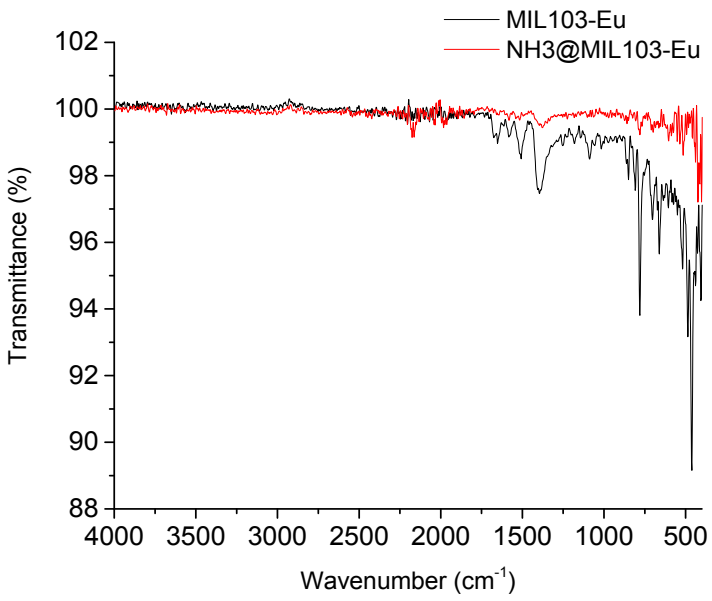

Figure S18. FTIR spectra of MIL103-Eu before and after 6 hour of NH_3 adsorption (NH_3@MIL103-Eu).

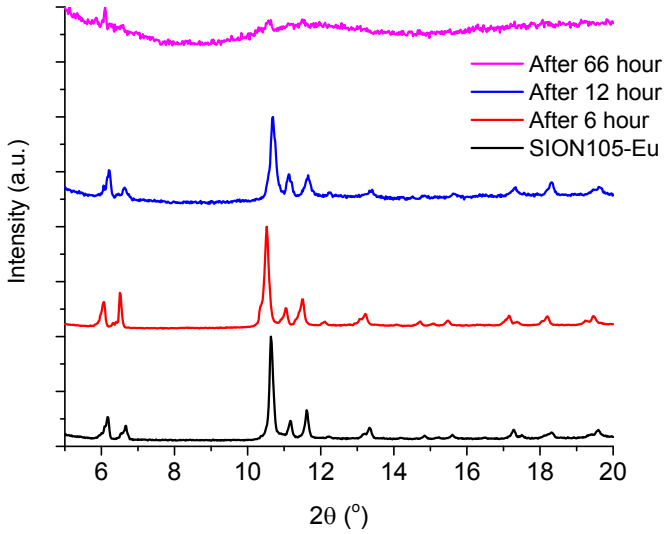

Figure S19. PXRD patterns of **SION105-Eu** and the heated samples at 75 °C after 6, 12, and 66 hours of continuous adsorption of NH_3 vapor.

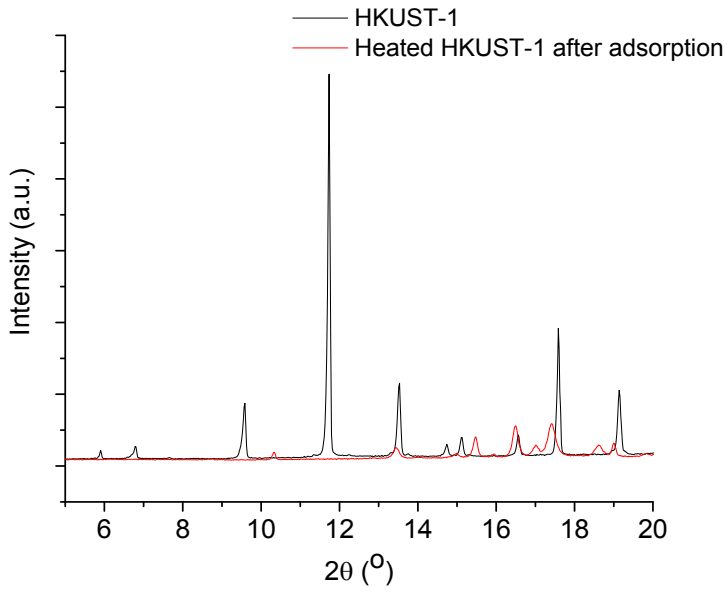

Figure S20. PXRD patterns of the as-made HKUST-1 and the heated sample at 75 °C after 1 hour of NH_3 vapor adsorption.

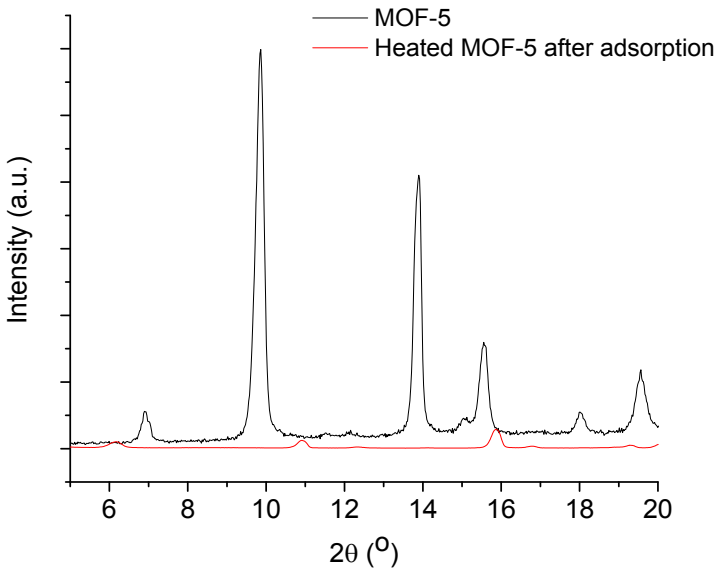

Figure S21. PXRD patterns of the as-made MOF-5 and the heated sample at 75 °C after 1 hour of NH_3 vapor adsorption.

Density Functional Theory Calculations

We performed first-principles density functional theory (DFT) calculations a plane-wave basis and projector augmented-wave (PAW)[3-4] pseudopotentials with the Vienna ab-initio Simulation Package (VASP) code.[5-8] To include the effect of the van der Waals (vdW) dispersive interactions on binding energies, we performed structural relaxations with revised vdW-DF2 method[9] as implemented in VASP. For all calculations, we used a Γ-point sampling of the Brillouin zone and (ii) a 500 eV plane-wave cutoff energy. The Hubbard U of 9.1 eV and J of 0.7 eV on Eu 4*f* states were chosen on the basis of previous first-principles calculations.[10] We used ferromagnetic ordering along the metal oxide chain direction (*b*-axis) and antiferromagnetic ordering between two Eu atoms in the chains. According to our DFT calculations, this magnetic structure is most stable among four candidates (see Figure S22 and Table S1). We explicitly treated nine valence electrons for Eu ($4f^7 6s^2$), six for O ($2s^2 2p^4$), four for C ($2s^2 2p^2$), three for B ($2s^2 2p^1$), and one for H($1s^1$). All structural relaxations were performed with a Gaussian smearing of 0.05 eV[11] while fixing the experimental lattice parameters. The ions were relaxed until the Hellmann-Feynman forces are less than 0.01 eVÅ^{-1}.

To compute the NH_3 binding energy, we optimized SION-105-Eu MOF prior to NH_3 adsorption ($E_{\text{SION-105-Eu MOF}}$), interacting with NH_3 in the gas phase (E_{NH3}) within a 20 Å × 20 Å × 20 Å cubic supercell, and SION-105-Eu MOF with adsorbed NH_3 molecule ($E_{\text{NH}_3\text{–SION-105-Eu MOF}}$) using a rigid MOF. The binding energies (E_{B}) are obtained via the difference

$$E_B = E_{NH_3 - SION - 105 - Eu\,MOF} - \left(E_{SION - 105 - Eu\,MOF} + E_{NH_3}\right). \quad (1)$$

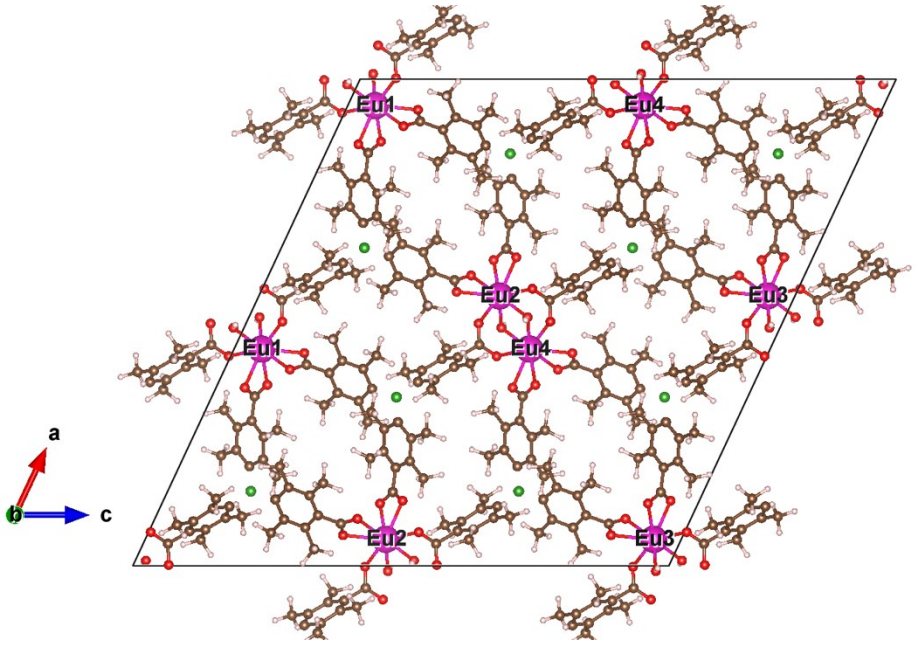

Figure S22. Optimized crystal structure of **SION-105-Eu** and its four different Eu sites. The image of the crystal structure was generated using the VESTA program.[12]

Table S1. Computed energies of ferromagnetic (FM) and different antiferromagnetic (AFM) orderings.

Magnetic configurations of Eu atoms	Energy (eV per formula unit)
FM (↑↑↑↑)	2.351
AFM1 (↑↓↓↑)	0.020
AFM2 (↑↑↓↓)	0.000
AFM3 (↑↓↑↓)	0.006

Table S2. Representative MOFs reported in the literature for NH_3 capture.

MOF	Capacity (mmol/g_{MOF}) at 1 bar, 298 K		Analysis Method	Ref
	Dry NH_3	Moist NH_3		
MOF-5 (Zn)	0.35		Break-through	[13]
IRMOF-62 (Zn)	1.35		Break-through	[13]
MOF-177 (Zn)	2.47		Break-through	[13]
MOF-199 (Cu)	5.11		Break-through	[13]
MOF-74 (Zn)	5.47		Break-through	[13]
IRMOF-3 (Zn)	6.17		Break-through	[13]
ZIF-8 (Zn)	1.0		Adsorption isotherm	[14]
MIL-53 (Al)	3.6		Adsorption isotherm	[14]
Al-BTB	5.7		Adsorption isotherm	[14]
MOF-74 (Mg)	13.9		Adsorption isotherm	[14]
HKUST-1 (Cu)	6.6	8.9	Break-through	[15]
UiO-66 (Zr)	1.79	2.75	Break-through	[16]
UiO-66-OH (Zr)	5.69	2.77	Break-through	[16]
Zn-BTTB	4.59	20.26	Break-through	[16]
DMOF-A (Zn)	0.48	1.18	Break-through	[16]
DMOF-TM2 (Zn)	0.15	4.57	Break-through	[16]
$Zn(INA)_2$	6.0	6.0	Gravimetric	[17]
SION-10 (Cu)	27.3		Break-through	[18]
Co_2Cl_2BBTA	17.95		Adsorption isotherm	[19]
Ni_2Cl_2BBTA	14.68		Adsorption isotherm	[19]
Cu_2Cl_2BBTA	19.79		Adsorption isotherm	[19]
MFM-300(Al)	13.9		Adsorption isotherm	[20]
$Co(NA)_2$	17.5		Adsorption isotherm	[21]
$Cu(NA)_2$	13.4		Adsorption isotherm	[21]
$Cd(NA)_2$	6.0		Adsorption isotherm	[21]
$Co_4(IDC)_4(pda)_4$	17.63		Adsorption isotherm	[22]
		4.73	Titration	
MIL-101 (Cr)	10.0		Adsorption isotherm	[23]
Al-PMOF	7.67		Adsorption isotherm	[24]
Ga-PMOF	10.50		Adsorption isotherm	[24]
In-PMOF	9.41		Adsorption isotherm	[24]
CPM-100a-FeNi	13.01		Adsorption isotherm	[25]
SION105-Eu	5.7[a]		Adsorption isotherm	This work
		5.9	Gravimetric	
[a] Measured at 1 bar, 303 K				

References

1. Shyshkanov, S.; Nguyen, T. N.; Ebrahim, F. M.; Stylianou, K. C.; Dyson, P. J., In Situ Formation of Frustrated Lewis Pairs in a Water-Tolerant Metal-Organic Framework for the Transformation of CO2. *Angew. Chem. Int. Ed.* **2019,** *58*, 5371-5375.
2. Ebrahim, F. M.; Nguyen, T. N.; Shyshkanov, S.; Gładysiak, A.; Favre, P.; Zacharia, A.; Itskos, G.; Dyson, P. J.; Stylianou, K. C., Selective, Fast-Response, and Regenerable Metal–Organic Framework for Sampling Excess Fluoride Levels in Drinking Water. *J. Am. Chem. Soc.* **2019,** *141*, 3052-3058.
3. Blöchl, P. E., Projector augmented-wave method. *Physical Review B* **1994,** *50*, 17953-17979.

4. Kresse, G.; Joubert, D., From ultrasoft pseudopotentials to the projector augmented-wave method. *Phys. Rev. B* **1999,** *59*, 1758-1775.
5. Kresse, G.; Hafner, J., Ab initio molecular dynamics for liquid metals. *Phys. Rev. B* **1993,** *47*, 558-561.
6. Kresse, G.; Furthmüller, J., Efficient iterative schemes for ab initio total-energy calculations using a plane-wave basis set. *Phys. Rev. B* **1996,** *54*, 11169-11186.
7. Kresse, G.; Furthmüller, J., Efficiency of ab-initio total energy calculations for metals and semiconductors using a plane-wave basis set. *Comput. Mater. Sci.* **1996,** *6*, 15-50.
8. Kresse, G.; Hafner, J., Ab initio molecular-dynamics simulation of the liquid-metal--amorphous-semiconductor transition in germanium. *Phys. Rev. B* **1994,** *49*, 14251-14269.
9. Hamada, I., van der Waals density functional made accurate. *Phys. Rev. B* **2014,** *89*, 121103.
10. Nilsson, F.; Sakuma, R.; Aryasetiawan, F., Ab initio calculations of the Hubbard U for the early lanthanides using the constrained random-phase approximation. *Phys. Rev. B* **2013,** *88*, 125123.
11. Elsässer, C.; Fähnle, M.; Chan, C. T.; Ho, K. M., Density-functional energies and forces with Gaussian-broadened fractional occupations. *Physical Review B* **1994,** *49*, 13975-13978.
12. Momma, K.; Izumi, F., VESTA: a three-dimensional visualization system for electronic and structural analysis. *J. Appl. Crystallogr.* **2008,** *41*, 653–658.
13. Britt, D.; Tranchemontagne, D.; Yaghi, O. M., Metal-organic frameworks with high capacity and selectivity for harmful gases. *Proc. Natl. Acad. Sci. U. S. A* **2008,** *105*, 11623-11627.
14. Kajiwara, T.; Higuchi, M.; Watanabe, D.; Higashimura, H.; Yamada, T.; Kitagawa, H., A Systematic Study on the Stability of Porous Coordination Polymers against Ammonia. *Chem. Eur. J.* **2014,** *20*, 15611-15617.
15. Peterson, G. W.; Wagner, G. W.; Balboa, A.; Mahle, J.; Sewell, T.; Karwacki, C. J., Ammonia Vapor Removal by Cu3(BTC)2 and Its Characterization by MAS NMR. *J. Phys. Chem. C* **2009,** *113*, 13906-13917.
16. Jasuja, H.; Peterson, G. W.; Decoste, J. B.; Browe, M. A.; Walton, K. S., Evaluation of MOFs for air purification and air quality control applications: Ammonia removal from air. *Chem. Eng. Sci.* **2015,** *124*, 118-124.
17. Chen, Y.; Yang, C.; Wang, X.; Yang, J.; Ouyang, K.; Li, J., Kinetically controlled ammonia vapor diffusion synthesis of a Zn(ii) MOF and its H2O/NH3 adsorption properties. *J. Mater. Chem. A* **2016,** *4*, 10345-10351.
18. Gładysiak, A.; Nguyen, T. N.; Navarro, J. A. R.; Rosseinsky, M. J.; Stylianou, K. C., A Recyclable Metal–Organic Framework as a Dual Detector and Adsorbent for Ammonia. *Chem. Eur. J.* **2017,** *23*, 13602-13606.
19. Rieth, A. J.; Dincă, M., Controlled Gas Uptake in Metal–Organic Frameworks with Record Ammonia Sorption. *J. Am. Chem. Soc.* **2018,** *140*, 3461-3466.
20. Godfrey, H. G. W.; da Silva, I.; Briggs, L.; Carter, J. H.; Morris, C. G.; Savage, M.; Easun, T. L.; Manuel, P.; Murray, C. A.; Tang, C. C.; Frogley, M. D.; Cinque, G.; Yang, S.; Schröder, M., Ammonia Storage by Reversible Host–Guest Site Exchange in a Robust Metal–Organic Framework. *Angew. Chem. Int. Ed.* **2018,** *57*, 14778-14781.
21. Chen, Y.; Shan, B.; Yang, C.; Yang, J.; Li, J.; Mu, B., Environmentally friendly synthesis of flexible MOFs M(NA)2 (M = Zn, Co, Cu, Cd) with large and regenerable ammonia capacity. *Journal of Materials Chemistry A* **2018,** *6*, 9922-9929.
22. Chen, Y.; Wang, Y.; Yang, C.; Wang, S.; Yang, J.; Li, J., Antenna-Protected Metal–Organic Squares for Water/Ammonia Uptake with Excellent Stability and Regenerability. *ACS Sustainable Chemistry & Engineering* **2017,** *5*, 5082-5089.
23. Chen, Y.; Zhang, F.; Wang, Y.; Yang, C.; Yang, J.; Li, J., Recyclable ammonia uptake of a MIL series of metal-organic frameworks with high structural stability. *Microporous and Mesoporous Materials* **2018,** *258*, 170-177.

24. Moribe, S.; Chen, Z.; Alayoglu, S.; Syed, Z. H.; Islamoglu, T.; Farha, O. K., Ammonia Capture within Isoreticular Metal–Organic Frameworks with Rod Secondary Building Units. *ACS Mater. Lett.* **2019,** *1*, 476-480.
25. Wang, Y.; Zhao, X.; Yang, H.; Bu, X.; Wang, Y.; Jia, X.; Li, J.; Feng, P., A Tale of Two Trimers from Two Different Worlds: A COF-Inspired Synthetic Strategy for Pore-Space Partitioning of MOFs. *Angew. Chem. Int. Ed.* **2019,** *58*, 6316-6320.